Energy 353 (2026) 141016

Contents lists available at ScienceDirect

Energy

journal homepage: www.elsevier.com/locate/energy

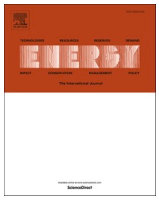

Performance assessment of air-to-water heat pumps in alpine regions under present and future climate: Impacts of start-up and defrosting cycles

Fabian Eze *, Maja Danovska, Vittoria Benedetti, Alessandro Prada

Department of Civil, Environmental and Mechanical Engineering, University of Trento, Via Mesiano 77, 38123, Trento, Italy

ARTICLE INFO

Keywords:
Air-water heat pump
Startup time
Defrosting cycle
Climate change
Heating and cooling

ABSTRACT

Air-to-water heat pump (AWHP) is a key technology for decarbonising building heating, yet their deployment in Alpine regions remains limited due to performance degradation at low source temperatures. These regions are climate-change hot-spots characterised by rapid warming and complex topography, raising the question of whether future climate change will alleviate or intensify the operational constraints affecting AWHPs. This study quantifies the combined impact of start-up and defrosting losses on AWHP performance under present and future climate conditions. An integrated TRNSYS-based model was developed, incorporating experimentally derived degradation correlations for start-up and defrosting cycles. A single-family house equipped with an inverter-driven AWHP was simulated for five Alpine municipalities in Northern Italy, across elevations from 83 to 652 m above sea level. In the base year, start-up operation accumulates up to 40 to 70 h per month during transitional and winter periods, while defrosting reaches up to 30 to 40 cycles per month at higher elevations. These transient effects reduce the seasonal coefficient of performance (SCOP) by 4 to 6% due to start-up alone and up to 11% when combined with defrosting, leading to primary energy increases of 7 to 12%. By 2050, climate warming reduces defrosting frequency by up to 33 to 100% in transitional months, while start-up hours remain significant due to increased part-load operation. As a result, SCOP increases by about 2% in 2030 and 6% in 2050, with primary energy consumption decreasing by up to 10%. Explicit modelling of operational dynamics is essential for realistic AWHP assessment.

Abbreviations and Symbols

Abbreviations	Meanings
ASHP	Air-source heat pump
AWHP	Air-water-heat pump
BESS	Battery energy storage system
COP	Coefficient of performance
DHW	Domestic hot water
EER	Energy efficiency ratio
HVAC	Heating, ventilation, and air-conditioning
PE	Primary energy
PTES	Pumped thermal electricity storage
PV	Photovoltaic
RH	Percentage relative humidity (%)
SCOP	Seasonal coefficient of performance (−)
SEER	Seasonal energy efficiency ratio (−)
Ssf	Steady-state frequency (Hz)
TES	Thermal energy storage
Symbols	
T_{air}	Ambient air temperature (°C)
DT	Temperature difference between the supply temperature and the setpoint (°C)
e	Water vapor pressure (Pa)
e_s	Saturated water vapor pressure (Pa)
$T_{d,corr}$	Corrected dew point temperature (°C)
T_x and $\overline{T}$	Maximum temperature and mean temperature (°C)
α	Temperature calibration coefficient (−)
$COP_{actual,d}$	Actual COP of HP during defrosting cycle (−)
$COP_{actual,s}$	Actual COP of HP during start-up time (−)
P_{actual}	Actual power consumption of ASHP (kW)
$\dot{Q}_{heating/cooling}$	Heat transfer rate for heating or cooling (kW)
E_{grid}	Energy imported from the grid (kWh)
E_{pv}	Energy produced from PV and consumed (kWh)
f_{grid}	Primary energy conversion factor for electricity from grid (i.e., 2.43 for Italy)
f_{pv}	Primary energy conversion factor for electricity from PV (i.e., 1 for Italy)
$t_{start-up}$	Start-up time (minutes)

* Corresponding author.
E-mail addresses: fabianchidubem.eze@unitn.it, fabianchidubem@gmail.com (F. Eze).

https://doi.org/10.1016/j.energy.2026.141016
Received 4 February 2026; Received in revised form 16 March 2026; Accepted 9 April 2026
Available online 13 April 2026

1. Introduction

The increasing global emphasis on sustainable and energy-efficient heating and cooling in buildings has led to a growing interest in the air-water heat pumps (AWHPs) for residential and commercial applications [1]. AWHP is a type of air-source heat pump (ASHP), where air is utilized on the source-side while delivering heat to water on the sink-side at a predefined temperature range [2]. Although all ASHPs utilise air as the heat source, air-to-air heat pumps transfer heat directly to indoor air, whereas AWHP uses water as the heat transfer medium, enabling integration with hydronic systems such as underfloor heating, radiators, and thermal storage tanks [3]. In Europe, the application of this system is essential in achieving the global Net-Zero target proposed by the European Commission, aiming at decarbonisation and a consequent reduction in building energy bills by 2030, in line with the European Green Deal of zero net emissions of greenhouse gases by 2050 [4] [5]. Indeed, AWHPs are characterized by high efficiencies with seasonal coefficient of performance (SCOP) values ranging from 3.5 to over 6, depending on system design and operating conditions [6]. Moreover, these systems enable the integration of renewable energy sources, such as solar, to meet the thermal energy demands for efficient domestic hot water (DHW) heating and building space conditioning applications [7]. For example, the application of solar-assisted AWHP could balance photovoltaic (PV) power generation and consumption by consuming the power produced directly during periods of high demand and charging the storage systems when little or no heating demand is required for later use. Despite these advantages, AWHP performance often degrades due to varying environmental conditions and operational dynamics [8], particularly in regions, like the Alps, characterised by low temperatures in winter, rapid warming, and complex topography [9]. Among the key factors influencing this performance are the startup cycles [10] and defrosting cycles [11]. During start-up, the system often operates less efficiently as it needs to overcome the initial thermal inertia, introducing thermal and mechanical stress that may also shorten the component lifespan [12]. A study by Zhang et al. [10] found that startup losses are due to mechanical and thermal delays, which reduce the overall system performance. It showed that the AWHP is capable of maintaining continuous refrigerant cycles at low compressor frequencies, thereby improving average thermal efficiency by 26.42%. These system behaviour is more common in the Alps, where rapid changes in weather are often encountered [13]. Similarly, in humid and cold environments, often seen in typical Alpine regions, frost accumulates on the outdoor heat exchanger of the heat pump, necessitating a defrosting cycle to maintain efficient performance [11,14]. These dynamic behaviours are also emphasised by the recurring type of detached timber buildings, due to their low thermal inertia, and high performance building due to their low heating demand [15]. The operations, though temporary, can recur frequently in locations with mild and extreme climate conditions, affecting the system performance, which significantly impacts the energy efficiency, compressor reliability, and user comfort [16]. However, these aspects have often been neglected in the dynamic simulation of heat pumps for water and space heating, leading to possible over-estimation of their performance. Only a limited number of studies in the literature have attempted to investigate those aspects, in particular, with the aim of ascertaining the impact of dynamic behaviours and frost formation on heat pump performance, as well as to recommend potential mitigation strategies, using a variety of methodological approaches. This highlights a gap in current modelling approaches and the need for more comprehensive analyses that account for real operating conditions.

1.1. Previous study on start-up dynamics

Regarding the impact of dynamic behaviours, Zhao et al. [17] investigated and observed that an ASHP with variable speed compressors could mitigate some of the startup inefficiencies by allowing a smoother transition from off to operational states. This smoother startup process reduces mechanical stress and allows for better energy management, improving efficiency during normal operation. Their results demonstrated that a R290-based system could reduce the energy consumption associated with startup compared to traditional systems with fixed-speed compressors. Oehler et al. [18] proposed a strategy for modulating heat pump start-up, including quick traverses of the compressor's natural frequencies. The frequency modulation enhanced the performance of the heat pump, confirming its importance. Similarly, Lu et al. [19] investigated the performance of a large-scale pumped thermal electricity storage during start-up cycles, discovering that the rate of rotational speed affects the start-up time, which degrades the system performance. Furthermore, Kumar et al. [20] developed an integrated thermodynamic model for a reversible AWHP, analysing both variable-speed and constant-speed compressors. The study investigates the transient operation during startup phases and explores control strategies to enhance system efficiency and stability. Their findings indicate that optimizing startup control can significantly improve the coefficient of performance (COP), with potential increases ranging from 17% to 50%.

1.2. Previous study on defrosting cycles

Defrosting methods, including reverse-cycle defrosting, often cause temporary drops in the COP of the heat pump, negatively affecting the heating supply [21]. Few studies have explored the formation processes of frost in ASHP and proposed innovative ways to minimize defrost cycles to improve performance. Ma et al. [22] developed a numerical model for investigating this aspect that was validated using experimental data. The authors reported an agreement between the developed model and the experimental data with a normalized error residue of 0.025. Using TRNSYS and with site-measured data, Rossie Di Schio et al. [23] modelled a system that examined the impact of defrosting cycles on the performance of ASHP during the heating period, reporting that neglecting the defrosting cycle losses results in an inaccurate prediction of its performance, and is capable of reducing the SCOP by 10%. Since frost build-up on the external heat exchanger of AWHP impacts negatively on their performance, Eze et al. [24] developed a shallow underground thermal storage (UTS), where cold or warm heat can be stored and extracted for preheating and precooling of the inlet air to the heat pump [7]. This study showed that by preheating the inlet air and raising the temperature from −15 °C to temperatures above 10 °C using the UTS, the SCOP during heating was improved by 9% compared to a conventional case without preheating. Similarly, Li et al. [25] investigated a thermal energy storage (TES)-based defrosting method for ASHP. Analysis of the system energetic and economic feasibility highlighted that the TES-based approach can enhance heating efficiency from 3.0% to 19.5% compared to the conventional case, although its integration increases the overall capital costs. The impact of defrosting cycles on ASHP, especially in cities with mild and extreme weather conditions, extends to overall electricity demand. For example, Milev et al. [26] developed a Simulink model to investigate the impact of defrosting cycles based on the weather conditions of 10 cities around the world. The study produced a validated model that can estimate power demand across various climatic conditions by predicting the frequency of defrosting cycles with ambient temperature conditions.

1.3. Research gaps and objectives of the study

It is evident from past studies that the start-up delays and defrosting cycles can degrade the performance of AWHPs by 3 - 15%, depending on climatic conditions. Despite their significant influence, these factors remain insufficiently quantified in dynamic simulations that are typically used to evaluate seasonal performance. Even with the existing few studies, the investigations relied on white-box models, where system behaviour is represented using physical models but without explicitly

integrating real-world performance dynamics [24]. This oversight contributes to a persistent gap between simulated results and the actual operational performance of AWHPs. Modelling start-up time poses particular challenges because it depends strongly on the inverter's steady-state frequency (ssf). Accurate correlations linking start-up time, ssf, temperature difference, and the resulting COP degradation must therefore be established experimentally. Similarly, defrosting-related efficiency losses can only be quantified through experimental measurements, as they are highly sensitive to dry-bulb temperature and relative humidity. Without integrating such experimentally derived correlations, simulation tools like TRNSYS cannot fully capture the practical performance of AWHPs, including the control strategy, under any given climatic conditions and heat pump operating frequencies. Failing to properly model these aspects can undermine the reliability of scenario analyses such as designing solutions that are resilient to climate change. In Europe, it is almost certain that the performance of AWHPs and their deployment in their vast Alpine regions with severe dynamic weather conditions will be significantly affected [27–29]. Northern part of Italy, particularly the Trentino region is characterized by this complicated weather conditions, with municipalities located at significant varying elevations, adding complexities in the projection of climate change and its impacts to energy systems such as AWHP. Some studies, as seen in Refs. [30–33], have investigated the impacts of climate change on the water-energy-food-ecosystem nexus in this region, with the aim of understanding the dynamics and proposing future solutions. A study by Congedo et al. [34] has already shown on a global scale that the rise in temperature will have significant impact on the performance of ASHP, but this study was not extended to Alpine regions characterized by mountains and lowlands. Of course, defrosting and its impact on energy efficiency is one factor that limits the diffusion of AWHP in Alpine regions, even though they have been identified as a key measure for decarbonizing the building heating sector in the Provincial Energy and Environmental Plan (PEAP). The question remains: to what extent will climate change affect these aspects while considering system transient behaviour? So far, this question is yet to be answered. In fact, and to the best of our knowledge, there has not been any study of this kind particularly for assessment of the long-term systems performance in the Alpine regions.

To address this gap, the present study developed an integrated modelling framework that explicitly incorporates previously derived and validated start-up and defrosting performance degradations correlations into TRNSYS simulations. The approach is applied to a case study in the Autonomous Province of Trento (Northern Italy), where complex alpine climate conditions present unique challenges for estimating building heating and cooling demands. Beyond current state-of-the-art studies, this work also incorporates long-term climate projections up to 2050 for five municipalities at different elevations, using measured data from local meteorological stations. These forecasts were employed to assess how future climate scenarios will influence AWHP performance in these regions, thereby providing a comprehensive evaluation of both present-day and future operational conditions.

2. Methodology

The study is focused on evaluating the integrated influence of startup time and defrosting cycles on the AWHP model and assessing its future performance under climate change scenarios in the Alpine regions. To this end, an integrated impact assessment model was developed using TRNSYS (v.18), coupling the AWHP with a photovoltaic (PV) system, the electricity grid, a battery energy storage system (BESS), conventional thermal storage tanks, and a single-family house building model (see Figs. 1 and 2). The interactions among the components are governed by optimized control logics that determine when and under what conditions each system component operates. The model incorporates heat pump performance degradation curves accounting for defrosting and start-up cycles obtained from previous experimental work [35]. With the completion of the system architecture, five Municipalities in the Trentino region were selected. These municipalities are classified as mixed humid climate, referred to as the ASHRAE climate zone 4A. The historic weather data were obtained from local meteorological stations together with climate projections to 2030 and 2050 [36]. The impacts of these factors (defrosting and startup delays) on the performance of the AWHP under these projected climate conditions were evaluated, using 2016 data as the base year, while applying different temperature boundary conditions. The performance assessments under these scenarios were based on performance indicators such as the COP, SCOP, Energy Efficiency Ratio (EER), seasonal EER (SEER), and the annual primary energy (PE) consumption, defined explicitly in section 2.3.

2.1. Climate condition prediction

To predict the heat pump performance under changing climate conditions, ambient air temperature (T_{air}) and relative humidity (RH) were predicted for 2030 and 2050 using climate data obtained from five municipalities (Arco, Trento, Storo, Cavedine and Cles) of the Trentino Province, as shown in Fig. 3, with different elevations of 83, 185, 384, 549, and 652 in meters, respectively. These municipalities were selected since they represent the complex climate hotspots where the dynamic operation of AWHP is heavily affected due to startup and defrosting dynamics.

Meteorological data included hourly values of T_{air}, RH, and solar irradiance. From these measured temperatures, the future weather data were generated based on the Test Reference Years derived from historical data, applying a hybrid projection model that combines dynamic downscaling and the morphing technique described fully in Laiti et al. [37]. By using the projected daily hourly temperature (T_{air}), it was

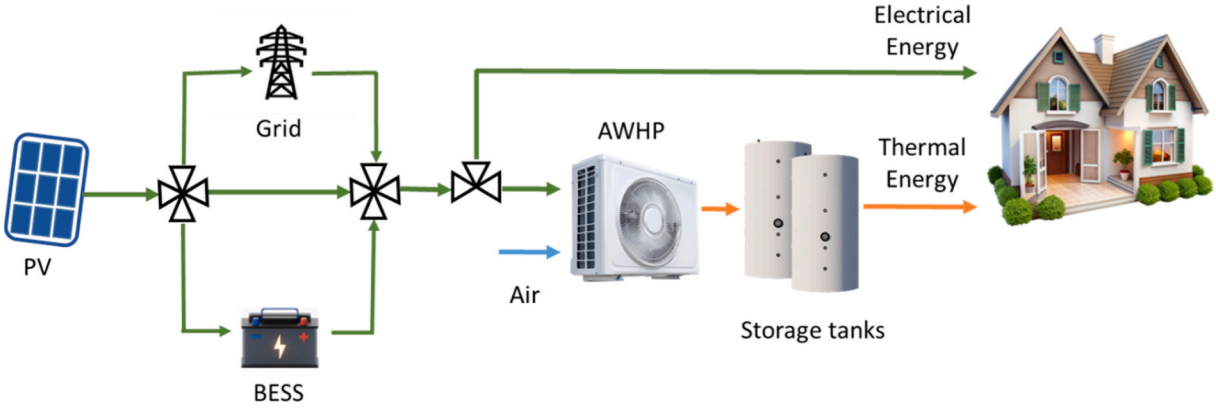

Fig. 1. System configuration.

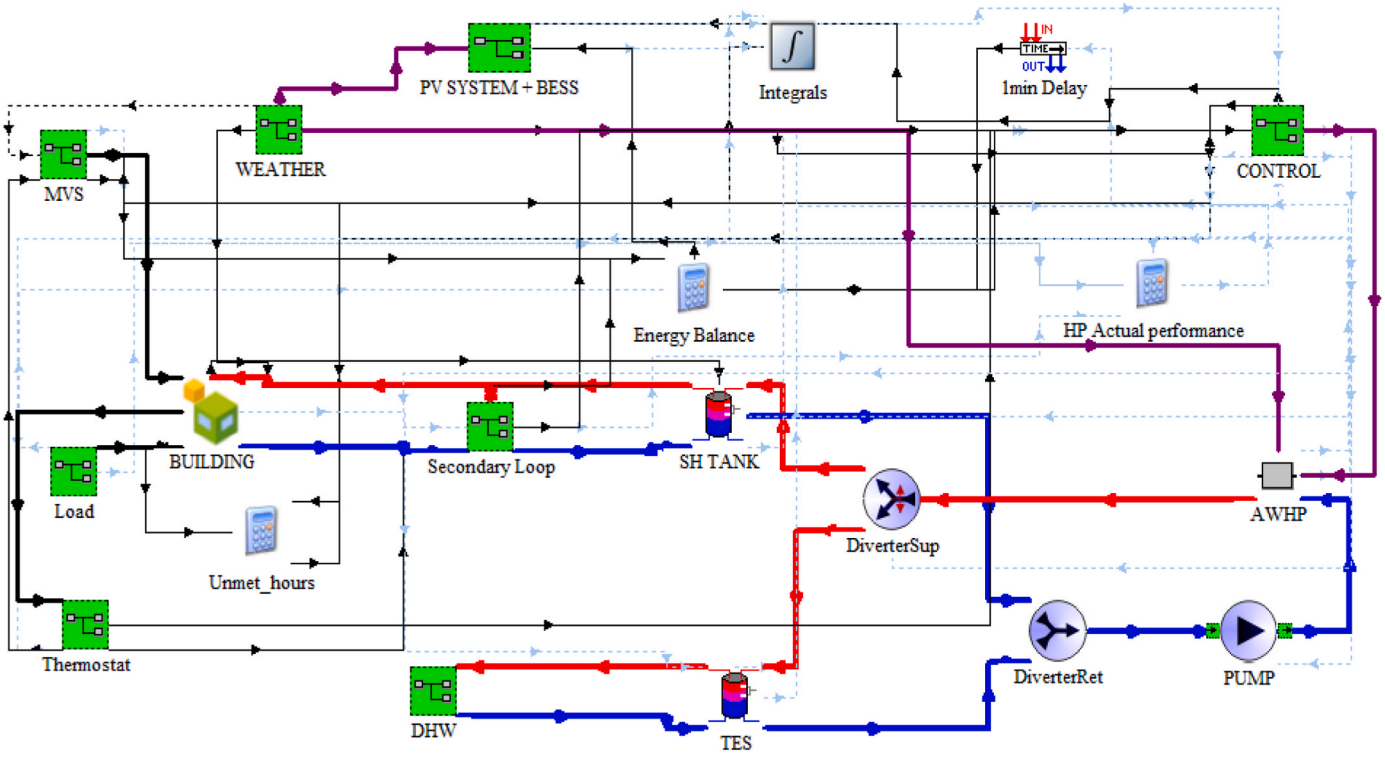

Fig. 2. Layout of the developed TRNSYS model.

Fig. 3. Geographical location of the study site (Arco = 83 m, Trento = 185 m, Storo = 384 m, Cavedine = 549 m and Cles = 652 m).

possible to estimate the projected RH according to Eq. (1), approximating the minimum temperature as a first guess and its correction factors, as described in the approach developed and validated by Eccel et al. [38].

$$RH = 100\frac{e}{e_s} \tag{1}$$

where e_s (saturated water pressure) and e (water vapor pressure) are calculated via empirical correlations as shown in Eq. (2) and Eq. (3):

$$e_s = 6.1078\ exp^{7.5\left(\frac{T_{air,min}}{T_{air}+273.3}\right)} \tag{2}$$

$$e = 6.1078\ exp^{7.5\left(\frac{T_{d,corr}}{T_{d,corr}+273.3}\right)} \tag{3}$$

where $T_{air,min}$ is the air temperature corresponding to the daily minimum value, evaluated assuming that the water vapor in the atmosphere is saturated at the temperature corresponding to the dew point, and $T_{d,corr}$ is the corrected dew point calculated via Eq. (4), where α is the calibration coefficient equal to 0.1, T_x and $\overline{T}$ are the daily maximum and mean temperature, respectively.

$$T_{d,corr} = T_{air,min} - \alpha\left(0.45(T_x - \overline{T}) + \overline{T} - T_{air,min}\right) \tag{4}$$

2.2. Model component description

2.2.1. Building model

The building under investigation is a single-family residential dwelling with a total heated floor area of 140 m^2 divided into four thermal zones, two for each floor. The selected building type and its thermal properties is the most adopted residential building in the study region. The share of single-family and terraced houses among residential buildings ranges from 87% in Trento to 99% in Storo, according to census data used in the Provincial Energy and Environmental Plan [39]. The geometry and thermal properties of the building envelope were defined in the TRNBuild environment, and it was subsequently integrated into the TRNSYS Simulation Studio via Type56. The thermal transmittance (U-values) of the envelope components were set equal to 0.65 W m^{-2} K^{-1} for the external walls, 0.52 W m^{-2} K^{-1} for the ground floor, 0.63 W m^{-2} K^{-1} for the roof and 0.86 W m^{-2} K^{-1} for the glazed components of the envelope to simulate a typical existing domestic building.

2.2.2. Heat pump model

The building is equipped with a R32 inverter-driven AWHP with specifications of 8.73 kW and 9 kW rated cooling and heating capacities, respectively, which corresponds to a 2.11 kW and a 1.89 kW cooling and heating power absorption, necessary for both space heating, cooling, and DHW production. The AWHP was developed and validated by Roccatello et al. [40] to simulate its dynamic behaviour, which is dependent on the air temperature, air flow rates, water temperature, and flow rates. The heat pump model incorporates the modulation of the compressor speed through the steady-state frequency (ssf), which typically explains the operating frequency once stable conditions are reached. In this study, minimum, maximum, and nominal inverter frequencies of 15 Hz, 52 Hz, and 50 Hz were chosen with a maximum rate of frequency variation over each simulation time-step given as 20 Hz/min based on the applied control strategy implemented by the manufacturer. The heat pump was modelled through a customized subroutine type, and its operational behaviour was characterized using heating and cooling performance maps within predefined constraints. The outdoor temperature reset curve for heating is constrained within a matrix of minimum and maximum water temperature of 25 °C and 65 °C, respectively, corresponding to minimum and maximum air temperature of 20 °C and −20 °C. Similarly, the outdoor temperature reset curve for cooling was constrained within a matrix of minimum and maximum water temperatures of 7 °C and 25 °C, respectively, which corresponds to a minimum and maximum air temperatures of 46 °C and 10 °C. In addition, a 1.0 kW backup resistance heater was integrated to help in meeting the supply setpoint temperature of the heat pump. The system performance, including the COP and the EER under nominal and part-load conditions, was constrained to operate within these natural variables. In addition, the climate data used (historical and projected scenarios) were evaluated within these operating ranges, and therefore no significant extrapolation beyond the validated model limits was required. The customized AWHP subroutine computes the electrical power $\dot{P}$ knowing the nominal thermal capacity, $\dot{Q}$, and the corresponding nominal COP using Eq. (5).

$$\dot{P} = \frac{\dot{Q}}{COP_{nominal}} \tag{5}$$

The delivered heat for heating or cooling ($\dot{Q}_{heating/cooling}$) is limited to the nominal capacity, $\dot{Q}$ based on the performance map and the operating constraints. However, if $\dot{Q}_{heating/cooling}$ is less than the load requirement, the unmet load is supplied through the buffer tank, whose temperature is maintained at setpoint through the backup resistance heater.

2.2.2.1. Start-up and defrosting modelling. To investigate the influence of startup and defrosting cycles, the study adopted correlations derived from experimental data and validated by Roccatello et al. [35]. The functions were experimentally obtained by testing an inverter-driven AWHP, at first, under transient conditions to assess the performance drop due to start-up phase up to 20 min ($COP_{d,s}$). After that, the same heat pump was tested under controlled environmental conditions T_{air} ranging from −4 to +4 °C and RH ranging from 70 to 90%, to quantify the performance drop due to defrosting cycles ($COP_{d,d}$).

In this study, firstly the startup time was computed ($t_{start\text{-}up}$) as a function of *ssf* according to Eq. (6). Secondly, $COP_{d,s}$ was assessed through Eq. (7) based on the *ssf* and the temperature difference between the supply and set-point temperatures (DT) using the given constraint and the equation constants detailed in Table 1. These correlations were adopted only during the heat pump startup, thus, for times lower than the $t_{start-up}$.

$$t_{start-up} = -0.54 * ssf + 34.9 \quad R^2 = 0.96 \tag{6}$$

$$COP_{drop,s} = a + b * ssf + c * DT + d * ssf^2 + e * ssf * DT \tag{7}$$

at $ssf \geq 30Hz$ and start-up time 12 min for the application of Eq. 6.In TRNSYS, once the heat pump start event, t_{start}, occurs, the start-up time window defined by Eq. (8) is applied. Where the start-up duration $t_{start-up}$ in minutes is then calculated as a function of the ssf, previously defined in Eq. (6) as follows:

$$t < t_{start} + \frac{t_{start-up}}{60} \tag{8}$$

During this time interval, the $COP_{drop,s}$ is computed and after the start-up period ends, the heat pump resumes steady-state operation according to the performance maps. The COP reduction calculated with Eq. (7) is used to determine the actual electrical power absorbed during the start-up phase by modifying Eq. (5) as follows:

$$\dot{P}_{actual} = \frac{\dot{Q}}{COP_{nominal}\left(1 + COP_{drop,s}\right)} \tag{9}$$

Based on the adopted correlations, it is assumed that the storage tanks and thermostat deadbands do not directly alter the start-up duration rather they affect the frequency of compressor cycling and consequently the number of start-up events.

Similarly, $COP_{drop,d}$ was modelled according to Eq. (10) as a function of RH and T_{air}, with equation constants given in Table 1. Generally in the operation of ASHPs, defrosting cycles are likely to occur at T_{air} below 3 °C and RH higher than 70% [41], therefore, these values were utilized in the present study for simulation and evaluation.

$$COP_{drop,d} = a + b * RH + c * T_{air} + d * RH * T_{air} + e * {T_{air}}^2 + f * RH * {T_{air}}^2 + g * {T_{air}}^3 \tag{10}$$

Where Eq. (10) is constrained to $T_{air} \leq 3$ °C and $RH \geq 70\%$ after the initial operation delay time of the heat pump. In the TRNSYS routine, a defrost event is permitted only when the climatic frosting condition is satisfied and the compressor is ON. At the start of the simulation, a time delay of 1 h was implemented, using component Type661 to prevent

Table 1
Correlation constants.

Constants	For $COP_{drop,s}$	For $COP_{drop,d}$
A	−107.7	15.05
B	1.907	−0.2543
C	21.16	0.01351
D	−0.002337	−0.007022
E	−0.3976	0.4319
F	-	−0.005945
G	-	0.03681

immediate trigger of the defrost event, however, the elapse time between two consecutive defrost cycles is not limited by any control and is therefore governed solely by the climatic and operating. This single defrost trigger criterion is used in case studies to conform with the experimental procedure adopted and for a fair comparison of the system performance.

Once the COP reduction is calculated with Eq. (10), the actual power absorbed by the heat pump is determined through the following equation:

$$\dot{P}_{actual} = \frac{\dot{Q}}{COP_{nominal}(1 + COP_{drop.d})} \quad (11)$$

2.2.3. Description of other system components

Two stratified thermal storage tanks, one for space heating/cooling (SH tank) and the other for DHW (TES tank), were included and modelled using Type60 from the TRNSYS component library. Storage tank volumes were equal to 277 L and 156 L, respectively. The DHW demand was set equal to 186 L per day based on the Italian technical specification UNI/TS 11300 [42], with a daily profile retrieved from EN 12831-3 [43]. It is important to note that when a defrost event or startup delays is activated, the model applies the COP degradation factors to the heat pump. In case of a temporary reduction in the delivered useful heating or when the supply temperature at setpoint cannot be maintained due to these effects, compensation is obtained from the buffer tank with the backup heater, exactly as in normal capacity limited periods. This ensures that indoor setpoint control remains consistent while the energy penalty of degraded operation is captured.

Moreover, the building model also incorporates a mechanical ventilation system (MVS) that includes a dehumidifier (Type14), a cross flow air-to-air heat recovery unit (Type667), and two mixing valves (Type648). Solar radiation was calculated using the Perez model (Type16), enabling an accurate representation of gains due to the solar radiation. Weekday and weekend-specific occupancy profiles were applied [44]. The appliance loads were modelled using stochastic demand profiles derived from measured household electricity consumption data [45]. These profiles capture realistic variations in appliance usage frequency, duration, and power levels, while preserving the statistical characteristics of daily and weekly energy demand. Distinct patterns were applied for weekdays and weekends to reflect differences in occupancy-related activities. The resulting appliance load profiles provide time-resolved electricity demand and contribute to the overall building energy balance as internal electrical loads, affecting both total electricity consumption and internal heat gains. The system also includes PV panels and a BESS of 3 kWh capacity. The PV array was modelled with Type94, by using 9 modules with a total nominal peak power of 4 kWp. The inverter efficiency was set equal to 97.3%. The BESS with charging and discharging efficiency of 0.9 was modelled based on the state of charge or discharge and the transient capacity degradation over the operational period as presented by Alic et al. [46]. The Energy regulation of the BESS operates based on the priority set by the employed control algorithm. In this control, the PV system generates energy and supplies it to the load. If this load is fully met and surplus PV power exists, the battery is prioritized, and the charging activates if within the capacity limit of 3.5 kW, 16 A, 220 V. If the battery is fully charged, surplus power is then exported to the grid. Additionally, if the PV power is not sufficient, battery discharging is activated until a 20% capacity threshold based on the control algorithm.

2.3. Key performance indicators

Performance of the heat pump based on the integrated impacts of startup and defrosting cycles was evaluated using key performance indicators described in Table 2. Once the percentage reduction was evaluated as a function of T_{air} and RH (for the defrost effect) and as a function of the heat pump on/off state (for the start-up degradation), the performance of the heat pump was modified and either the COP or the EER were updated inside the customized subroutine type. The actual COP due to defrosting cycles and startup time were calculated using Eqs. (11) and (12), respectively. Obtaining the actual power consumption of the heat pump with Eq. (13), the SCOP and SEER, as shown in Eqs. (14) and (15), were calculated. The annual PE in Eq. (16) represents the total final energy consumption of the building over one year converted into primary energy by means of the primary energy factors. It includes energy imported from the grid, energy generated and consumed from the installed PV system, and energy supplied by the BESS to meet the building's thermal and electrical requirements. These requirements include the operation of the appliance load, heat pump, MVS, dehumidifier, and HVAC auxiliary systems. The electrical energy consumption of the heat pump for heating, cooling and DHW production was further used to calculate variations across different climate scenarios for the selected municipalities.

Table 2
Performance indicators.

Performance Indicator	Expression	Eqn No
Actual COP due to defrosting cycle	$COP_{actual,d} = COP_{nominal}(1 + COP_{drop,d})$	(11)
Actual COP due to start-up time	$COP_{actual,s} = COP_{nominal}(1 + COP_{drop,s})$	(12)
Actual power consumption of HP	$\dot{P}_{actual} = \frac{\dot{Q}_{heating/cooling}}{COP_{actual}}$	(13)
SCOP	$SCOP = \frac{\int_{t_i}^{t_f}(Q_{heating})dt}{\int_{t_i}^{t_f}(P_{actual})dt}$	(14)
SEER	$SEER = \frac{\int_{t_i}^{t_f}(Q_{cooling})dt}{\int_{t_i}^{t_f}(P_{actual})dt}$	(15)
Primary Energy (PE)	$\left(\sum_{n=1}^{N} E_{grid}\right) \times f_{grid} + \left(\sum_{n=1}^{N} E_{pv}\right) \times f_{pv}$	(16)

2.4. Limitations and assumptions

The results of this study should be interpreted considering several underlying assumptions. First, the performance degradation of the AWHP is represented through experimentally derived and validated correlations describing start-up and defrosting cycles obtained from previous experimental investigations. These validated performance degradation correlations are assumed sufficient for the study of future performance under various climate conditions. Second, the study is limited to a single-reference building (single-family house) with identical thermal properties (U-values) across all municipalities and climate scenarios to isolate the influence of climatic conditions on heat pump operation and for a fair comparative performance assessment of the case study sites. Consequently, the results are assumed to represent the behaviour of the investigated system configuration rather than the full diversity of building characteristics within the region. Furthermore, based on the adopted correlations, it is assumed that building thermal inertia, storage tanks, and thermostat deadbands do not directly modify the start-up duration; instead, these factors influence the steady-state compressor frequency and therefore the frequency of compressor cycling and the number of start-up events. In addition, defrost operation was represented using a simplified climatic criterion based on outdoor air temperature and relative humidity corresponding to the experimental frosting conditions under which the correlations were developed. Finally, the experimentally derived correlations are considered

sufficient for evaluating the operational behaviour and performance of the AWHP in the selected Alpine municipalities, although future studies may further benefit from site-specific monitored data for present-day comparison.

3. Results and discussion

3.1. Climate predictions

The impacts of projected climatic changes, specifically the changes in T_{air} and RH, on the operational performance of an AWHP were systematically analysed for the selected case study building and sites. The climate predictions raging between the minimum of −10 °C in winter and maximum of 34 °C in summer [37] for the selected municipalities indicated a consistent increasing trend up to the year 2050, with variations that correlate with elevation. These temperatures are within the operating constraints of the AWHP described in section 2.2.2. In Fig. 4, the average temperature rise, corresponding to their elevations above the sea level is shown for the year 2030 and 2050. An upward trend in the rise of temperature will be observed however, this increment did not exceed 1.5 °C in all municipalities as demonstrated in where the average temperature rise across all the Municipalities are presented. Between the base year (2016) and 2030, the increase in average air temperature is minimal, ranging from 0.48 °C in Arco to 0.60 °C in Cles. By 2050, however, the warming becomes more noticeable, with projected increases of 1.24 °C in Arco and 1.50 °C in Cles. These values indicate a steady upward trajectory in average temperatures, reflecting broader global climate change scenarios. However, the cities would remain within the limited temperature rise of 2 °C based on the Paris agreement. Considering the different elevations, a clear relationship can be observed between elevation and temperature rise. Municipalities at higher altitudes, such as Storo, Cavedine, and Cles, are projected to experience greater increases compared to their lowland counterparts, Arco and Trento. For instance, Cles, situated at 652 m above sea level, shows the highest temperature rise, whereas Arco at 83 m registers the lowest. This elevation-sensitive and expected rise in temperature over time shows the vulnerability of alpine regions, where relatively small shifts in temperature may have significant effects on energy demand, especially in the built environments.

3.2. Impacts of climate changes on the heat pump operation

3.2.1. Startup time

Startup events introduce recurring transient operating conditions that significantly influence the real-world operation of AWHP, particularly in climates with strong thermal variability such as the Alpine region. During the simulation, the variation of the ssf modulated the compressor speed of the heat pump to balance load demand. At low ssf, the compressor speed is lowered, reducing the power input, but also extending the start-up time. The reverse is the case with high load demand, when the compressor ramps up more quickly, shortening start-up time but increasing mechanical and thermal stress. This is evident from Fig. 5, which demonstrate the monthly startup time in hours for the municipalities with the lowest (83 m) and highest (652 m) elevations, representing Arco and Cles, respectively. The result data for other municipalities are presented in Table A.1 of the appendix section. In the base year, the startup times reveal a pronounced seasonal pattern across all five municipalities. As shown in Fig. 5a and b, the startup time remained consistently low by approximately 6 h per month in summer. This consistently low startup hours can be attributed to the large capacity of the TES and the buffer tank for DHW and cooling, respectively. In contrast, this does not occur during winter operation, given the greater severity of the climate, which benefits the startup cycles. In winter and transitional months higher startup times were obtained, with maximum occurring in March by approximately 70 h and secondary peaks in October and November by approximately 40 to 58 h. These periods correspond to frequent on–off cycling caused by fluctuating heating loads and rapidly changing outdoor temperatures, which repeatedly force the AWHP into transient operations.

The projected changes for 2030 and 2050 indicate that startup behaviour remains sensitive to future climatic conditions based on the assumptions that the temperatures used to calculate the design load remain unchanged and the size of the heat generator remains accurate. By 2050, Arco with the lowest elevation will experience an increase in the startup times by up to 20% in winter and by up to 6% in summer when compared with the present day. Similarly, Cles with the highest elevation will experience an increased startup times of up to 25% in winter, which will be lowered to about 2% in summer. This suggests that future operation may be increasingly dominated by part-load conditions, where intermittent demand promotes cycling rather than continuous operation. Summer months already displayed small reductions or negligible changes in startup time, although the operational relevance of these variations is limited due to the already low absolute startup durations. The fact that in summer months, more stable operation is witnessed and the heat pump is utilized for DHW production and cooling, the warming temperature tends to reduce impacts of the climate changes on operational scale.

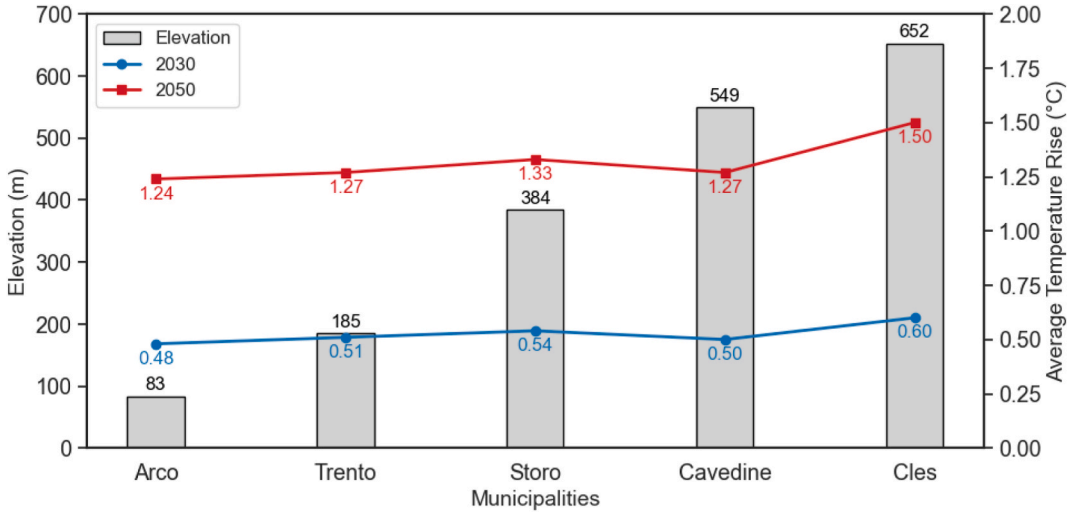

Fig. 4. Projected average temperature rise for the selected Municipalities at different elevations considering 2016 as the base year.

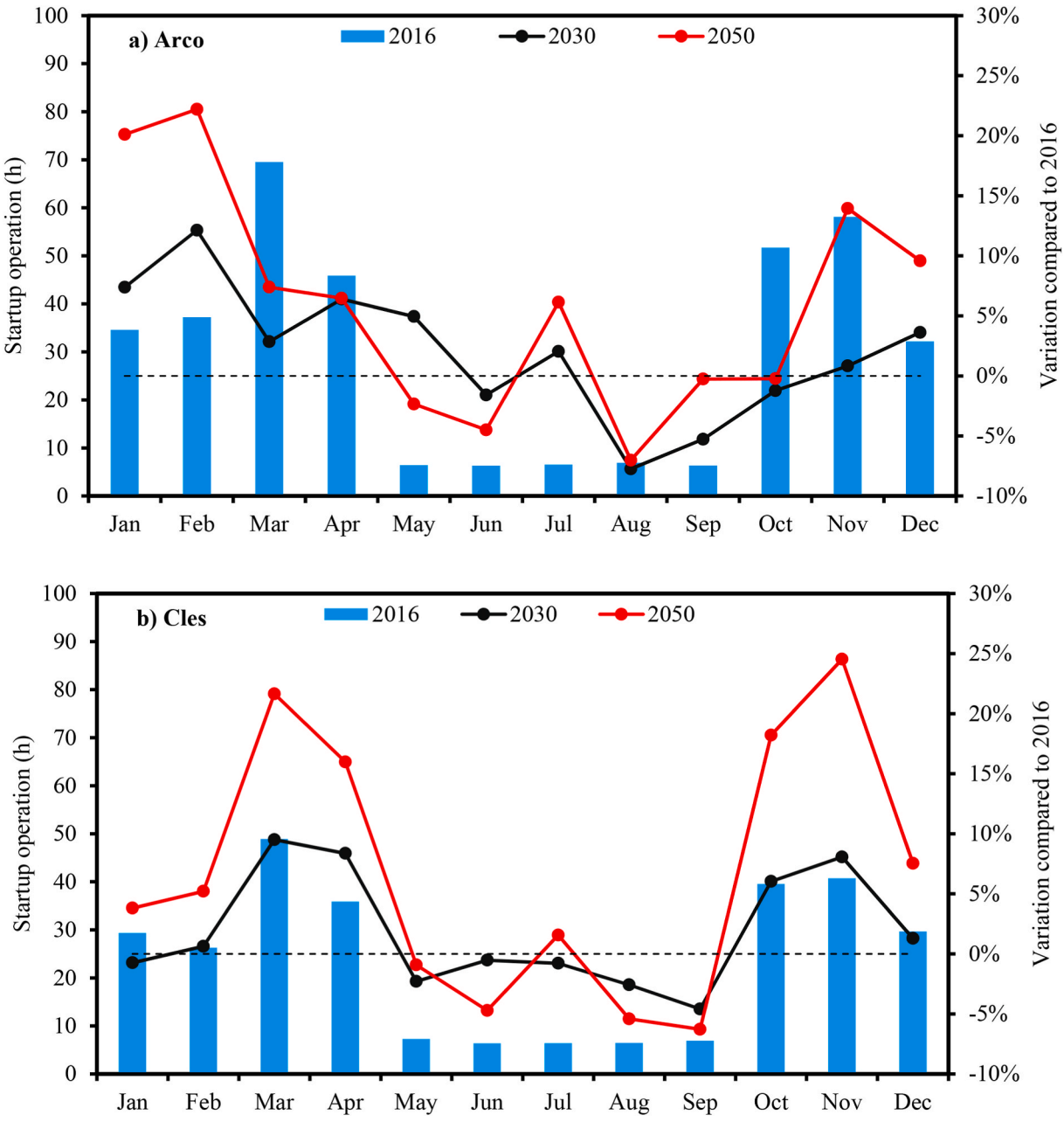

Fig. 5. Monthly startup time in hour for a) Arco with elevation 83 m and b) Cles 652 m.

3.2.2. Defrosting cycles

The impact of defrosting cycles on the AWHP is demonstrated in Fig. 6 for Arco and Cles with similar patterns for other municipalities represented in Table A.2 of the appendix section. In the base year, defrosting events are concentrated in cold months and are entirely absent from May to September as expected. In the present day as shown in Fig. 6 a), defrosting cycles occur repeatedly within a single month, reaching up to 31 cycles in January and 34 cycles in December for Arco. In Cles (Fig. 6 b), the number of cycles recorded 42 and 28 for January and December, respectively. This is a demonstration that at higher elevation, lowered T_{air} and high RH will have operational impacts on the AWHP. In mountainous climates such as this region, the heat pump will frequently be forced into non-heating operational modes during peak demand periods, which may affect the building occupants.

Projected climate data for 2030 and 2050 show a general reduction in defrosting frequency during late winter and early spring. In Arco, the defrosting cycles will experience a decrease by up to 10% in 2030 and up 33% by 2050, and even up 100% for the month of October when compared with the present-day scenario. In Cles with high elevation, the defrosting cycles will extend to the months of April and May unlike in the lower elevation. This site will experience a decrease by up to 50% and 100% in 2050, particularly in April. These changes indicate a contraction of the frost-active operating window, which reduces the cumulative number of defrost interruptions during winter seasons. However, mid-winter months display more heterogeneous trends. Generally, in January and December, defrosting cycles remained stable or even increase slightly at some locations particularly at higher elevations (Table A.2). The implication in these trends is that as the climate changes towards a more warming scenarios, the Alpine regions depending on elevations will experience a substantial reduction or total elimination of defrosting operation of the AWHP.

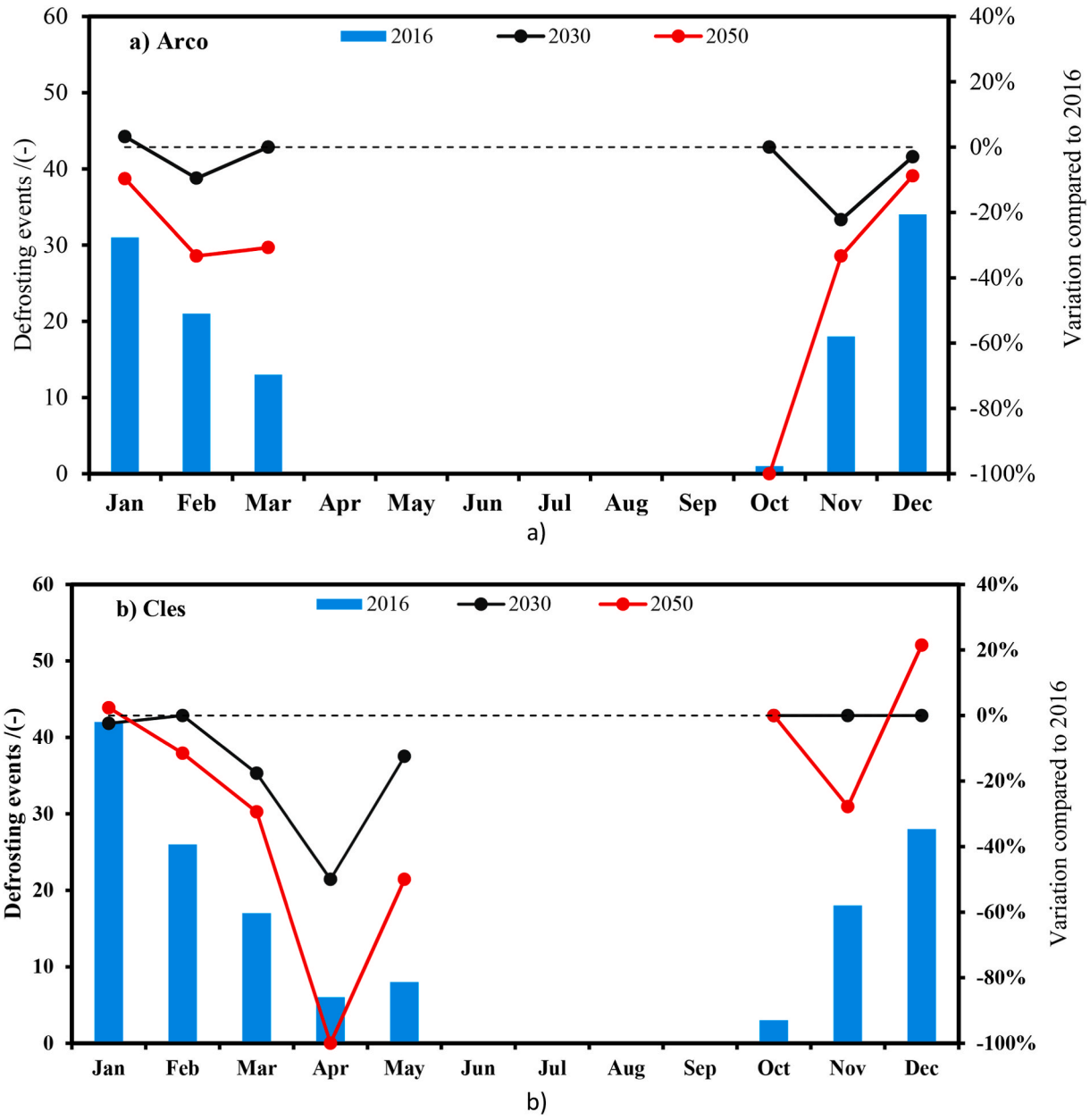

Fig. 6. Monthly startup time in hour for a) Arco with elevation 83 m and b) Cles 652 m.

3.3. Impact of startup and defrosting cycle on the AWHP performance

The quantified variations in seasonal performance indicators clearly illustrate how startup and defrosting dynamics translate into performances losses for AWHP as demonstrated in Fig. 7. These changes are highly dependent on the elevation of the municipality, climate, and the surrounding terrain. In the base year (Fig. 7a), startup effects alone reduce the SCOP by approximately 4 to 6.0% across all municipalities, while simultaneously maintaining a consistent increase in the annual PE consumption between 3.2 and 3.5%. The combined effects of startup delay and defrosting cycles significantly increased the drop in the SCOP by about 9 to 11% and consequent increase in the PE 7 to 12%. Although Arco's elevation is the lowest, the PE increased up to 12% with the combined effects of the startup and defrosting. This high PE increase in Arco could be attributed to its proximity to the Lake Garda, which may contribute to the frequent variation in the humidity. Trento on the other hand with high drop in the SCOP and lowest increase in the PE suggests more favourable conditions for heat pump operation during winter. With the decrease in SEER during summer by approximately 4 to 6%, Trento remained less affected decreasing by 4.2%.

In the 2030 scenario (Fig. 7b), startup-related impacts remain comparable to the base year. SCOP reductions due to startup alone range between 4.9 and 6.4%, with associated increases in annual PE consumption consistent between 3.3 and 3.7% across all municipalities. When startup and defrosting effects are combined, SCOP reductions remain intensified, reaching 9 to 11%, while PE penalties range from 5 to 8%. Compared to the base year, this represents a noticeable reduction in PE increase, particularly in lower-elevation sites such as Arco and Trento. This indicates that while startup-induced inefficiencies persist due to continued cycling and part-load operation, the reduced frequency of defrosting cycles in transitional months such as in March and April, partially mitigates their cumulative energy impact. By 2050 (Fig. 7c), the influence of startup delays becomes slightly more pronounced. Startup-related SCOP reductions increased to between 5 and 7%, reflecting a greater dominance of intermittent operation under milder but more variable heating conditions. However, the combined impact of

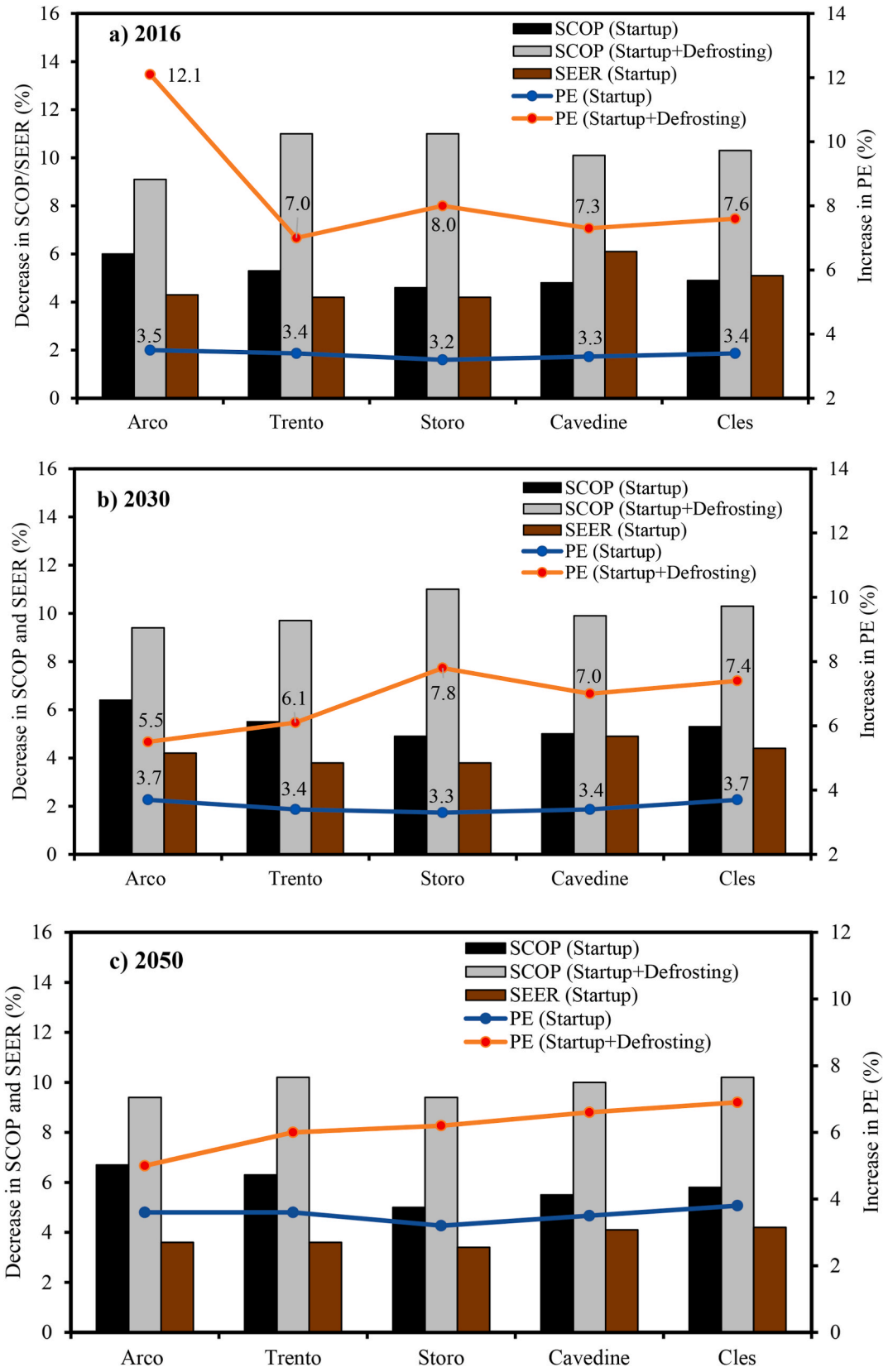

Fig. 7. Impact of defrosting and startup cycles on the performance of AWHP a) 2016 b) 2030, and c) 2050.

startup and defrosting stabilizes or slightly decreases compared to 2030, with SCOP reductions clustering around 9 to 10.2% and PE increments further declining between 5 and 7%. This trend suggests the possibility that continuous reductions in defrosting cycles offset the intensifying startup effects, leading to a redistribution rather than an amplification of seasonal losses.

In both 2030 and 2050, the impact on cooling performance remains modest. SEER reductions decrease progressively from the base year to 2030 and further to 2050, falling to approximately 3 to 4% by 2050. This confirms that future climate conditions reduce the sensitivity of cooling performance to transient effects, while heating performance remains strongly influenced by startup and defrosting dynamics. In addition, the simulated COP degradation associated with start-up and defrost events is consistent with the experimentally derived correlations reported by

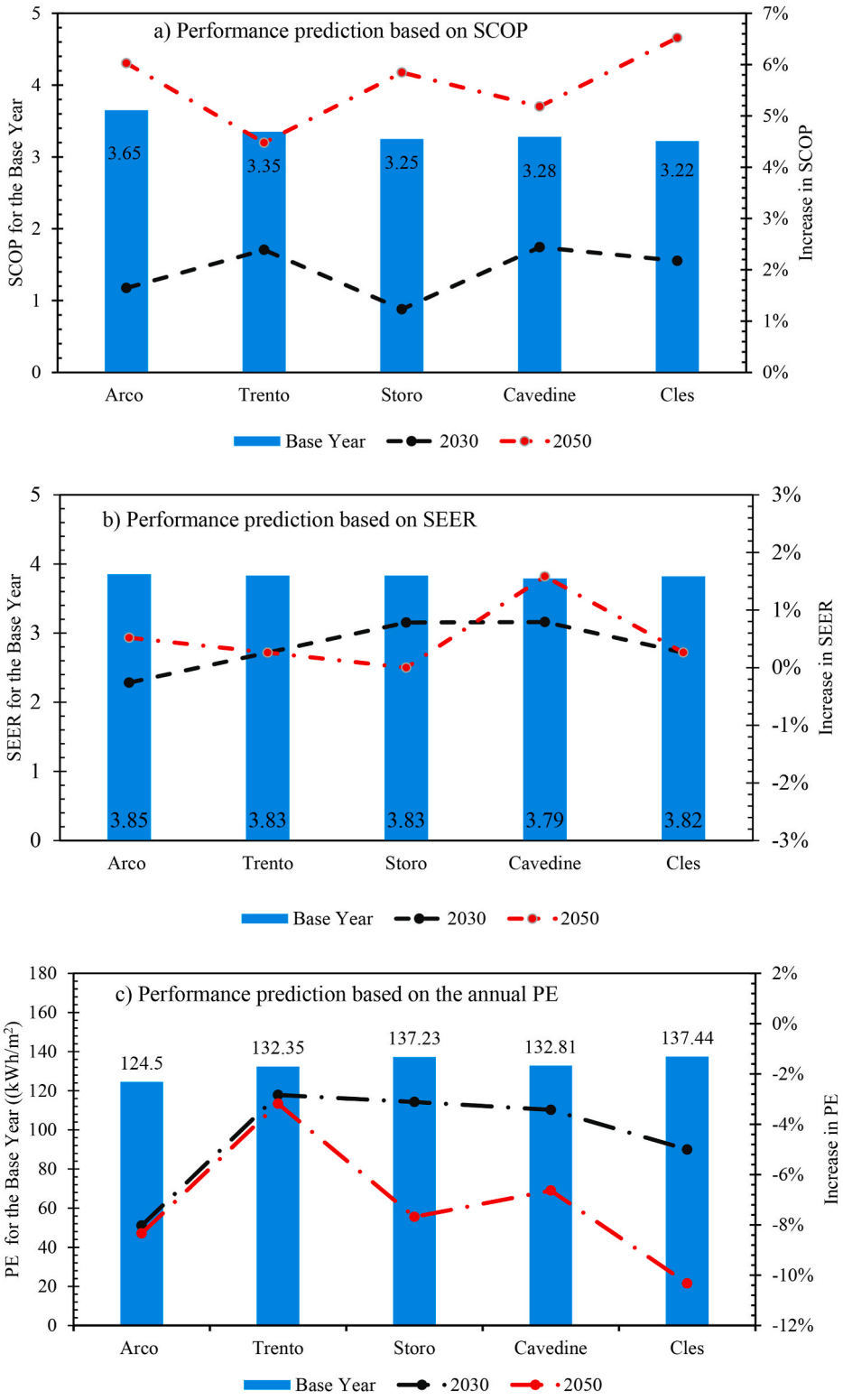

Fig. 8. Impact of climate change on the AWHP performance a) based on the SCOP b) based on the SEER and c) based on the annual PE consumption.

Roccatello et al. [35], from which the present degradation models were obtained. Furthermore, the predicted defrost patterns are physically consistent with Alpine climatic conditions, reported in Rossie Di Schio et al. [23], where outdoor temperatures frequently occur close to the freezing point combined with relatively high humidity, conditions known to favour frosting and defrost operation in ASHP.

3.4. Impact of climate changes on AWHP performances

To evaluate the impact of future climate changes on the AWHP performance, the combined effects of startup delays and defrosting cycles were considered to represent the actual behaviour of the system without over-estimation of results. Fig. 8 demonstrates the results obtained for the future performance based on the SCOP, SEER, and the annual PE consumption. In the base year, the SCOP ranged between 3.0 and 3.7 across all municipalities, as shown in Fig. 8a. Under future climate scenarios, the SCOP increases by an average of approximately 2% in 2030 and 6% in 2050, driven by a general warming trend. These results suggest that AWHP performance, particularly during heating operation, is likely to improve as the climate shifts toward warmer conditions. A lower risk of frost formation further contributes to this improvement, thereby enhancing the operational efficiency of heat pumps in mountainous regions.

This is further shown in Fig. 9, where the electrical consumption of the heat pump specifically for heating, cooling, and DHW production are demonstrated. Electrical demand for heating increases with elevation, however as the warming climate improves the performance, this demand decreases. For example, in Arco, the electrical consumption of the heat pump decreases by 4% in 2030 and by 8% by the end of 2050. This is a significant improvement because of climate change.

As shown in Fig. 8b, the SEER remained approximately constant across all municipalities in the base year. This can be attributed to the limited on–off cycling during periods when only DHW and cooling operation are required, which kept startup durations relatively stable. In 2030 and 2050 climate scenarios, the impact of climate change on SEER remains negligible, with SEER increasing up to 2% only in Cavedine by 2050. Although the projected changes in SEER are relatively small, Fig. 9 indicates that future climate conditions will lead to an increase in the heat pump's electrical demand for cooling. For instance, in Arco, the cooling power is projected to increase by approximately 2% in 2030 and by up to 6% in 2050.

The annual PE as shown in Fig. 8c indicated a fluctuating trend across the municipalities with Arco recording the lowest (124.5 kWh/m^2) and Cles recording the highest (137.44 kWh/m^2). However, as the climate changes, the heat pump operation improves and PE drops. For example, in 2030, the PE drops by up to 8% in Arco and by 5% in Cles, and by the end of 2050 Arco will experience a drop in PE slightly higher than 8% while in Cles, it will drop by up to 10%.

The expectation is that as the air temperature rises, the heating demand will reduce, leading to improvement in the SCOP. However, as the heating demand is reduced, cooling demand is expected to increase, although not observed as significant as the heating demand. It is an indication that the increase in the temperature rise within these Alpine municipalities will eventually offer a prevailing advantage to the AWHP. Further and explicit numerical results are presented in Table A.3 of the Appendix section.

4. Conclusion

This study quantified the operational and performance impacts of startup delays and defrosting cycles on air-to-water heat pumps operating in Alpine climates, under both current and future climate conditions. By integrating experimentally validated correlations into a TRNSYS simulation framework, the analysis explicitly captured transient behaviours that are typically neglected in seasonal performance assessments. However, the obtained results are subject to the few assumptions and limitations such as the absolute dependency on the experimentally derived and validated performance degradation correlations, the use of single representative building with the same thermal properties (U-values), single defrost triggering logic, and the AWHP startup dependency soley on the ssf.

The results demonstrate that startup and defrosting dynamics substantially affect AWHP operation. In the base year, startup operation accumulates primarily during winter and transitional months, reaching up to 70 h per month in March and 40 to 60 h in autumn months due to frequent on–off cycling under variable thermal loads. Defrosting cycles are concentrated in cold and humid periods, with up to 30 to 40 cycles per month observed at higher-elevation sites. These operational patterns are affected by elevation, climate conditions and site topography. From a performance perspective, the results demonstrate that transient behaviours significantly influence AWHP performance, particularly during heating operation. In the base year, startup delays alone reduce SCOP by up to 6%, while the combined effects of startup and defrosting cycles lead to SCOP reductions of 9–11% and corresponding increases in annual primary energy consumption of up to 12%. These impacts intensify with elevation, reflecting harsher climatic conditions and more

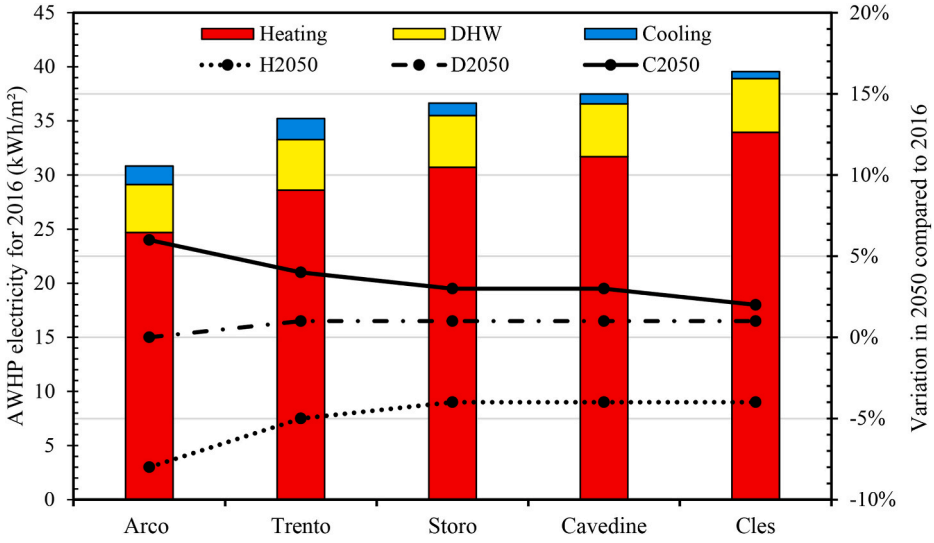

Fig. 9. Expected increase in the AWHP electrical demand specific for heating, cooling, and DHW production of the heat pump in 2050 compared to the base year.

frequent transient operation in higher-altitude municipalities. Cooling performance is comparatively less affected, as defrosting is absent and startup durations remain limited.

Future climate projections indicate that warming trends will partially offset these losses. Reduced frost occurrence leads to fewer defrosting cycles, while milder winter conditions improve overall heating efficiency. By 2050, SCOP increases by up to 6% and primary energy consumption decreases by up to 10% across the investigated sites, despite a slight increase in startup-related cycling under part-load conditions. Cooling demand and capacity increase modestly, but SEER remains largely unchanged. These findings confirm that accounting for startup and defrosting dynamics is essential for realistic long-term performance assessment of AWHPs, particularly in mountainous regions. The proposed modelling framework provides a robust tool for supporting climate-resilient system design, energy planning, and policy decisions aimed at accelerating the deployment of heat pumps in Alpine and similar climates. The imminent reduction in defrosting operations and the improvement in seasonal performance indicate that low ambient temperatures may become a less critical constraint for heat pump operations, thereby enhancing their technical feasibility and supporting wider adoption even in traditionally cold locations where performance limitations currently restrict their fully widespread. The current study has contributed in showing that climate change will moderately alleviate, but not fully resolve, the operational challenges of AWHPs in Alpine regions. Nevertheless, future studies should explore site-specific monitored data of defrost and start-up events for the same AWHP unit for further comparison of the predicted present-day cycle frequencies. Additionally, it may be necessary to extend the modelling framework to other building types such as multi-family residential and commercial buildings, where the influence of different load profiles and thermal inertia on start-up and defrost behaviours can be studied indepth.

CRediT authorship contribution statement

Fabian Eze: Writing – review & editing, Writing – original draft, Visualization, Software, Methodology, Formal analysis, Data curation, Conceptualization. **Maja Danovska:** Writing – review & editing, Writing – original draft, Visualization, Software, Methodology, Formal analysis, Data curation, Conceptualization. **Vittoria Benedetti:** Writing – review & editing, Visualization, Validation. **Alessandro Prada:** Writing – review & editing, Visualization, Validation, Supervision, Funding acquisition, Conceptualization.

Declaration of competing interest

The authors declare that they have no known competing financial interests or personal relationships that could have appeared to influence the work reported in this paper.

Acknowledgement

This research was funded by Fondazione CARITRO Cassa di Risparmio di Trento e Rovereto, grant number 2022.0239.

Appendix A

This section provides a detailed numerical result of this study. In Table A.1, monthly startup times in hours are shown while in Table A.2 the monthly number of defrosting cycles were detailed. Similarly, Table A.3, detailed the numerical result of the SCOP, SEER, and the annual PE were presented for all investigated scenarios.

Table A.1
Monthly startup time for all the investigated municipalities

Impact of Startup Time on the Operation of AWHP (Monthly startup time in hours and percentage change in 2030 and 2050)															
	Trento (height = 185m)			Storo (height = 384m)			Arco (height = 83m)			Cavedine (height = 549m)			Cles (height = 652m)		
	Base year	2030	2050	Base year	2030	2050	Base year	2030	2050	Base year	2030	2050	Base year	2030	2050
Jan	29.87	2%	7%	27.90	1%	3%	34.57	7%	20%	31.10	−6%	4%	29.35	−1%	4%
Feb	31.57	14%	17%	27.50	7%	19%	37.23	12%	22%	27.50	−3%	−1%	26.27	1%	5%
Mar	67.95	4%	6%	58.27	7%	22%	69.52	3%	7%	51.20	−7%	6%	48.90	10%	22%
Apr	42.75	4%	5%	49.58	0%	−2%	45.87	6%	6%	49.78	−1%	2%	35.87	8%	16%
May	6.85	−5%	−8%	6.85	3%	1%	6.40	5%	−2%	7.30	−3%	−7%	7.27	−2%	−1%
Jun	6.22	−1%	−1%	6.03	12%	−4%	6.30	−2%	−4%	6.27	5%	−3%	6.37	−1%	−5%
Jul	6.43	4%	−2%	5.98	6%	6%	6.52	2%	6%	6.15	0%	1%	6.38	−1%	2%
Aug	6.82	−4%	1%	6.18	−4%	−1%	6.88	−8%	−7%	6.33	0%	2%	6.47	−3%	−5%
Sep	6.43	2%	−8%	6.25	6%	1%	6.32	−5%	0%	6.82	0%	−5%	6.90	−5%	−6%
Oct	47.17	1%	7%	40.33	7%	5%	51.68	−1%	0%	44.18	−2%	−3%	39.53	6%	18%
Nov	49.67	6%	12%	53.30	1%	6%	58.08	1%	14%	51.98	−6%	8%	40.70	8%	25%
Dec	30.25	3%	7%	29.22	2%	4%	32.18	4%	10%	30.87	−4%	2%	29.65	1%	8%

Table A.2
Monthly defrosting cycles for all municipalities

Impact of Defrosting Cycles on the Operation of AWHP (Monthly number of cycles and percentage change in 2030 and 2050)															
	Trento (height = 185m)			Storo (height = 384m)			Arco (height = 83m)			Cavedine (height = 549m)			Cles (height = 652m)		
	Base year	2030	2050	Base year	2030	2050	Base year	2030	2050	Base year	2030	2050	Base year	2030	2050
Jan	38	3%	−8%	31.00	6%	10%	31.00	3%	−10%	40.00	3%	−8%	42.00	−2%	2%
Feb	18	0%	−6%	25.00	−8%	−8%	21.00	−10%	−33%	24.00	8%	−8%	26.00	0%	−12%
Mar	14	7%	−36%	22.00	−9%	−32%	13.00	0%	−31%	15.00	0%	0%	17.00	−18%	−29%
Apr	1.00	0%	0%	56.00	−20%	−39%	-	-	-	4.00	75%	−75%	6.00	−50%	−100%

(*continued on next page*)

Table A.2 (*continued*)

Impact of Defrosting Cycles on the Operation of AWHP (Monthly number of cycles and percentage change in 2030 and 2050)															
	Trento (height = 185m)			Storo (height = 384m)			Arco (height = 83m)			Cavedine (height = 549m)			Cles (height = 652m)		
	Base year	2030	2050	Base year	2030	2050	Base year	2030	2050	Base year	2030	2050	Base year	2030	2050
May	-	-	-	-	-	-	-	-	-	-	-	-	8.00	−13%	−50%
Jun	-	-	-	-	-	-	-	-	-	-	-	-	-	-	-
Jul	-	-	-	-	-	-	-	-	-	-	-	-	-	-	-
Aug	-	-	-	-	-	-	-	-	-	-	-	-	-	-	-
Sep	-	-	-	-	-	-	-	-	-	-	-	-	-	-	-
Oct	3.00	−67%	−100%	3.00	0%	−33%	1.00	0%	−100%	3.00	0%	33%	3.00	0%	0%
Nov	19.00	−11%	−16%	19.00	−5%	−16%	18.00	−22%	−33%	12.00	8%	−17%	18.00	0%	−28%
Dec	24.00	0%	0%	35.00	−17%	−11%	34.00	−3%	−9%	29.00	10%	0%	28.00	0%	21%

Table A.3
Elaborated Simulation results for all municipalities

Municipalities	SCOP without startup and defrosting	SCOP with Startup	SCOP with Startup + Defrosting	SEER Without startup	SEER with startup	PE Without startup and defrosting (kWh/m^2)	PE with Startup (kWh/m^2)	PE with Startup + Defrosting (kWh/m^2)
Base Year								
Arco	4.01	3.77	3.65	4.02	3.85	111.05	115.05	124.50
Trento	3.72	3.52	3.35	4.00	3.83	124.26	128.51	132.35
Storo	3.63	3.46	3.25	4.00	3.38	127.48	131.58	137.23
Cavedine	3.65	3.48	3.28	4.03	3.79	123.74	127.84	132.81
Cles	3.59	3.42	3.22	4.02	3.82	127.69	132.07	137.44
Year 2030								
Arco	4.10	3.84	3.71	4.01	3.84	108.57	112.57	114.51
Trento	3.80	3.59	3.43	3.99	3.84	121.18	125.25	128.60
Storo	3.70	3.52	3.29	4.01	3.86	123.38	127.45	132.96
Cavedine	3.73	3.54	3.36	4.02	3.82	119.84	123.97	128.26
Cles	3.67	3.47	3.29	4.01	3.83	121.54	126.06	130.56
Year 2050								
Arco	4.22	3.94	3.87	4.01	3.87	108.68	112.54	114.12
Trento	3.90	3.65	3.50	3.99	3.84	120.91	125.32	128.14
Storo	3.80	3.61	3.44	3.97	3.83	119.24	123.08	126.69
Cavedine	3.83	3.62	3.45	4.02	3.85	116.32	120.43	124.00
Cles	3.82	3.60	3.43	4.00	3.83	115.28	119.70	123.25

Data availability

Data will be made available on request.

References

[1] Li X, Sun Y, Wang W, Wei W. Enhancing demand response and heating performance of air source heat pump through optimal water temperature scheduling: method and application. Energy Build 2024;323:114839. https://doi.org/10.1016/j.enbuild.2024.114839.

[2] Wang R, Zhai X, editors. Handbook of energy systems in green buildings. Berlin, Heidelberg: Springer Berlin Heidelberg; 2017. https://doi.org/10.1007/978-3-662-49088-4.

[3] Christodoulides P, Christou C, Florides GA. Ground source heat pumps in buildings revisited and prospects. Energies 2024;17:3329. https://doi.org/10.3390/en17133329.

[4] O'Hegarty R, Kinnane O, Lennon D, Colclough S. Air-to-water heat pumps: review and analysis of the performance gap between in-use and product rated performance. Renew Sustain Energy Rev 2022;155:111887. https://doi.org/10.1016/j.rser.2021.111887.

[5] Renovation and decarbonisation of buildings. European Commission - European Commission n.d. https://ec.europa.eu/commission/presscorner/detail/en/ip_21_6683. [Accessed 15 April 2025].

[6] Mouzeviris GA, Papakostas KT. Study on air-to-water heat pumps seasonal performances for heating in Greece. Energies 2022;15:279. https://doi.org/10.3390/en15010279.

[7] Eze F, Lee W-J, An YS, Joo H, Lee K, Ogola J, et al. Development and simulated evaluation of inter-seasonal power-to-heat and power-to-cool with underground thermal storage for self-consumption of surplus solar energy in buildings. Energy Convers Manag 2024;320:119013. https://doi.org/10.1016/j.enconman.2024.119013.

[8] Xu Z, Zhao W, Shao S, Wang Z, Xu W, Li H, et al. Analysis on key influence factors of air source heat pumps with field monitored data in Beijing. Sustain Energy Technol Assessments 2021;48:101642. https://doi.org/10.1016/j.seta.2021.101642.

[9] Liu Z, Liu Y, Wu D, Jin G, Yu H, Ma W. Performance and feasibility study of solar-air source pump systems for low-energy residential buildings in Alpine regions. J Clean Prod 2020;256:120735. https://doi.org/10.1016/j.jclepro.2020.120735.

[10] Zhang D, Xinyue S, Pengfei L, Bo H, Gang H, Chunyang L, et al. Experiment study on startup characteristics and operation performance of PV/T solar assisted heat pump water heater system driven by direct current variable frequency compressor. Sol Energy 2023;263:111771. https://doi.org/10.1016/j.solener.2023.05.048.

[11] Ma J, Kim D, Braun JE, Horton WT. Development and validation of a dynamic modeling framework for air-source heat pumps under cycling of frosting and reverse-cycle defrosting. Energy 2023;272:127030. https://doi.org/10.1016/j.energy.2023.127030.

[12] Xu Z, Li H, Xu W, Shao S, Wang Z, Gou X, et al. Investigation on the efficiency degradation characterization of low ambient temperature air source heat pump under partial load operation. Int J Refrig 2022;133:99–110. https://doi.org/10.1016/j.ijrefrig.2021.10.002.

[13] Bellocchi S, De Iulio R, Guidi G, Manno M, Nastasi B, Noussan M, et al. Analysis of smart energy system approach in local alpine regions - a case study in Northern Italy. Energy 2020;202:117748. https://doi.org/10.1016/j.energy.2020.117748.

[14] Żelazna A, Pawłowski A. Review of the role of heat pumps in decarbonization of the building sector. Energies 2025;18:3255. https://doi.org/10.3390/en18133255.

[15] Figueiredo A, Almeida RMSF, Vicente R, Ferreira VM. Impact of heating strategies towards energy-efficient buildings. Energy Build 2024;315:114287. https://doi.org/10.1016/j.enbuild.2024.114287.

[16] Ma L, Sun Y, Wang F, Wang M, Zhang S, Wang Z. Advancements in anti-frosting and defrosting techniques for air source heat pumps: a comprehensive review of recent progress. Appl Energy 2025;377:124358. https://doi.org/10.1016/j.apenergy.2024.124358.

[17] Zhao Y, Du Y, Lin J, Guo N, Wu J. Start-up characteristics of a R290 rotary compressor for an air source heat pump under low ambient temperature condition. Int J Refrig 2024;159:385–94. https://doi.org/10.1016/j.ijrefrig.2023.12.021.

[18] Oehler J, Tran AP, Stathopoulos P. Simulation of a safe Start-Up maneuver for a Brayton heat pump. Volume 4: cycle innovations; cycle innovations: energy

storage. Rotterdam, Netherlands: American Society of Mechanical Engineers; 2022, V004T06A003. https://doi.org/10.1115/GT2022-79399.
[19] Lu C, Shi X, He Q, Liu Y, An X, Cui S, et al. Dynamic modeling and numerical investigation of novel pumped thermal electricity storage system during startup process. J Energy Storage 2022;55:105409. https://doi.org/10.1016/j.est.2022.105409.
[20] Kumar DM, Catrini P, Piacentino A, Cirrincione M. Integrated thermodynamic and control modeling of an air-to-water heat pump for estimating energy-saving potential and flexibility in the building sector. Sustainability 2023;15:8664. https://doi.org/10.3390/su15118664.
[21] Song M, Deng S. Defrosting for air source heat pump: research, analysis and methods. Duxford Cambridge, MA Kidlington: Woodhead Publishing; 2019.
[22] Ma J, Kim D, Braun JE. Transient simulation of an air-source heat pump under cycling of frosting and reverse-cycle defrosting. 2023. p. 26–37. https://doi.org/10.3384/ECP2118626.
[23] Rossi Di Schio E, Ballerini V, Dongellini M, Valdiserri P. Defrosting of air-source heat pumps: effect of real temperature data on seasonal energy performance for different locations in Italy. Appl Sci 2021;11:8003. https://doi.org/10.3390/app11178003.
[24] Eze F, Lee W, An YS, Joo H, Lee K, Ogola J, et al. Experimental and simulated evaluation of inverse model for shallow underground thermal storage. Case Stud Therm Eng 2024;59:104535. https://doi.org/10.1016/j.csite.2024.104535.
[25] Li Z-L, Zhang C-L, Liu H-M, Wang X-C. Feasibility analysis of thermal storage defrosting method for air source heat pump: from energetic and economic viewpoints. Appl Therm Eng 2024;236:121828. https://doi.org/10.1016/j.applthermaleng.2023.121828.
[26] Milev G, Al-Habaibeh A, Fanshawe S, Siena FL. Investigating the effect of the defrost cycles of air-source heat pumps on their electricity demand in residential buildings. Energy Build 2023;300:113656. https://doi.org/10.1016/j.enbuild.2023.113656.
[27] Masternak C, Meunier S, Reinbold V, Saelens D, Marchand C, Leroy Y. Potential of air-source heat pumps to reduce environmental impacts in 18 European countries. Energy 2024;292:130487. https://doi.org/10.1016/j.energy.2024.130487.
[28] Olympios AV, Justo Alonso M, Pantaleo AM. Heat pumps in Europe: perspectives and innovation challenges. Prog Energy 2025;7:032004. https://doi.org/10.1088/2516-1083/ade94a.
[29] Berta A, Gizzi M, Taddia G, Lo Russo S. The role of standards and regulations in the open-loop GWHPs development in Italy: the case study of the Lombardy and Piedmont regions. Renew Energy 2024;223:120016. https://doi.org/10.1016/j.renene.2024.120016.
[30] Carletti F, Michel A, Casale F, Burri A, Bocchiola D, Bavay M, et al. A comparison of hydrological models with different level of complexity in Alpine regions in the context of climate change. Hydrol Earth Syst Sci 2022;26:3447–75. https://doi.org/10.5194/hess-26-3447-2022.
[31] Cattivelli V. Climate adaptation strategies and associated governance structures in Mountain areas. The case of the alpine regions. Sustainability 2021;13:2810. https://doi.org/10.3390/su13052810.
[32] Orusa T, Borgogno Mondino E. Exploring short-term climate change effects on rangelands and broad-leaved forests by free satellite data in Aosta Valley (Northwest Italy). Climate 2021;9:47. https://doi.org/10.3390/cli9030047.
[33] Napoli A, Matiu M, Laiti L, Barbiero R, Bellin A, Zardi D, et al. Review on climate change impacts on the water-energy-food-ecosystems (WEFE) Nexus in the North-Eastern Italian alps. Clim Change 2025;178:41. https://doi.org/10.1007/s10584-025-03890-y.
[34] Congedo PM, Baglivo C, D'Agostino D, Mazzeo D. The impact of climate change on air source heat pumps. Energy Convers Manag 2023;276:116554. https://doi.org/10.1016/j.enconman.2022.116554.
[35] Roccatello E, Prada A, Baggio P, Baratieri M. Impact of startup and defrosting on the modeling of hybrid systems in building energy simulations. J Build Eng 2023;65:105767. https://doi.org/10.1016/j.jobe.2022.105767.
[36] Scarl O. Piano energetico ambientale provinciale 2021-2030. Provincia Autonoma Di Trento 2022. https://www.provincia.tn.it/Amministrazione/Documenti/Piano-Energetico-Ambientale-Provinciale-2021-2030. [Accessed 31 January 2026].
[37] Laiti L, Giovannini L, Zardi D. DOWNSCALING DI PROIEZIONI CLIMATICHE A SCALA LOCALE PER IL TERRITORIO DELLA PROVINCIA DI TRENTO AL 2030. Provincial Environmental Energy Plan 2021-2030 2019;Annex 2..
[38] Eccel E. Estimating air humidity from temperature and precipitation measures for modelling applications. Meteorol Appl 2012;19:118–28. https://doi.org/10.1002/met.258.
[39] Scarl O. Provincial environmental energy plan 2021-2030. Provincia Autonoma Di Trento; 2022. https://www.provincia.tn.it/en/Administration/Documents/Provincial-Environmental-Energy-Plan-2021-2030. [Accessed 16 March 2026].
[40] Roccatello E, Prada A, Baratieri M, Baggio P. Development of a detailed model of hybrid System composed by air-to-water heat pump and boiler. 2022. p. 540. https://doi.org/10.13124/9788860461919. x.
[41] Liang S, Wang H, Gao X, Tian X, Zhu H, Hu S, et al. Experimental study on the operating performance of the air source heat pump (ASHP) with variable outdoor airflow rate under the standard frosting condition. Energy and Built Environment 2024;5:719–26. https://doi.org/10.1016/j.enbenv.2023.06.001.
[42] UNI/TS 11300-2:2014 - UNI Italian standardization body 2014. https://store.uni.com/uni-ts-11300-2-2014. [Accessed 19 June 2025].
[43] EN 12831-3:2017 - energy performance of buildings - method for calculation of the design heat load - part 3: domestic hot water systems heat load and characterization of needs, Module M8-2, M8-3 n.d. https://store.uni.com/en-12831-3-2017 (accessed June 19, 2025).
[44] Besagni G, Premoli Vilà L, Borgarello M. Italian household load profiles: a monitoring campaign. Buildings 2020;10:217. https://doi.org/10.3390/buildings10120217.
[45] Povolato M, Prada A, Verones S, Baggio P. On the effect of the time interval base and home appliance on the renewable quota of a building in an alpine location. Energies 2022;16:384. https://doi.org/10.3390/en16010384.
[46] Alic A, Trovato V, De Paola A. Revenue maximization for a battery storage with optimal capacity revamping due to cyclic fade. IEEE Trans Smart Grid 2024;15:4779–91. https://doi.org/10.1109/TSG.2024.3391879.